

## Crystallization and thermomagnetic treatment of a Co-rich Co–Fe–Ni–Zr–B–Cu based nanocomposite alloy

P. R. Ohodnicki, Jr.,<sup>1,a)</sup> S. Y. Park,<sup>1</sup> D. E. Laughlin,<sup>1</sup> M. E. McHenry,<sup>1</sup> V. Keylin,<sup>2</sup> and M. A. Willard<sup>3</sup>

<sup>1</sup>Materials Science and Engineering Department, Carnegie Mellon University, Pittsburgh, Pennsylvania 15213, USA

<sup>2</sup>Magnetics, Division of Spang and Company, Pittsburgh, Pennsylvania 15238, USA

<sup>3</sup>Code 6355, Naval Research Laboratory, Washington, DC 20375, USA

(Presented on 6 November 2007; received 11 September 2007; accepted 30 October 2007; published online 4 March 2008)

The magnetic properties observed after various thermal-magnetic treatments for a  $(\text{Co}_{0.85}\text{Fe}_{0.15})_{83.6}\text{Ni}_{4.4}\text{Zr}_7\text{B}_4\text{Cu}_1$  alloy are compared with those for a  $(\text{Co}_{0.88}\text{Fe}_{0.12})_{79.4}\text{Nb}_{2.6}\text{Si}_9\text{B}_9$  alloy of similar Co:Fe ratio which exhibited a large field induced anisotropy in previous work. The qualitative conclusions arrived at here also apply to the  $(\text{Co}_{0.85}\text{Fe}_{0.15})_{88}\text{Zr}_7\text{B}_4\text{Cu}_1$  alloy without Ni. For the transverse magnetic field annealed  $(\text{Co}_{0.85}\text{Fe}_{0.15})_{83.6}\text{Ni}_{4.4}\text{Zr}_7\text{B}_4\text{Cu}_1$  alloy, the highest anisotropy fields  $H_K$  ( $H_K \sim 35\text{--}40$  Oe), field induced anisotropies  $K_U$  ( $K_U \sim 1700\text{--}2000$  J/m<sup>3</sup>), and lowest coercivities  $H_C$  ( $H_C \sim 0.5\text{--}1.5$  Oe at  $f=3$  kHz) were observed for field annealed amorphous ribbons as compared to field crystallized ribbons. For the  $(\text{Co}_{0.88}\text{Fe}_{0.12})_{79.4}\text{Nb}_{2.6}\text{Si}_9\text{B}_9$  alloy, the field induced anisotropy is a maximum for field crystallized ribbons ( $H_K \sim 28\text{--}45$  Oe,  $K_U \sim 800\text{--}1800$  J/m<sup>3</sup>) and the increase in dynamic coercivity ( $H_C \sim 0.5\text{--}1$  Oe at  $f=3$  kHz) observed upon crystallization is much less dramatic. The field annealed amorphous alloy of composition  $(\text{Co}_{0.85}\text{Fe}_{0.15})_{83.6}\text{Ni}_{4.4}\text{Zr}_7\text{B}_4\text{Cu}_1$  exhibited field induced anisotropies and dynamic coercivities that are competitive with the field crystallized alloys of composition  $(\text{Co}_{0.88}\text{Fe}_{0.12})_{79.4}\text{Nb}_{2.6}\text{Si}_9\text{B}_9$ . © 2008 American Institute of Physics. [DOI: 10.1063/1.2834400]

Fe, Co based nanocomposites can be engineered to exhibit excellent soft magnetic properties through averaging of the magnetocrystalline anisotropy of randomly oriented nanocrystals as described by the Herzer model.<sup>1</sup> Most attention has focused on Fe-rich alloys<sup>2,3</sup> or alloys near equiatomic Fe–Co ratios<sup>4</sup> due to their large saturation inductions, but Co-rich<sup>5–9</sup> and Ni-containing<sup>10,11</sup> alloys have been increasingly explored for technical applications and/or to study their crystallization and magnetic properties. In Co-rich Co–Fe–Nb–Si–B and Co–Fe–Zr–Si–B nanocomposite alloys, Yoshizawa *et al.* demonstrated a large field induced anisotropy and low losses for alloys with Co:Fe ratios of roughly 9:1 to 8:2.<sup>7,12</sup> The large field induced anisotropy was attributed to the formation of the nanocrystalline phase.

This work aims to contrast the magnetic properties observed after thermomagnetic treatment for a large field induced anisotropy Co–Fe–Nb–Si–B based alloy investigated previously by Yoshizawa *et al.*<sup>7,12</sup> and two Co–Fe–Zr–B–Cu based alloys synthesized here. Emphasis is placed on measuring the magnitude of the uniaxial field induced anisotropy constant  $K_U$  and the dynamic coercivity  $H_C$  observed after a number of transverse magnetic field annealing treatments.

Amorphous ribbons were melt spun using an overpressure of 1 psi of argon to eject the melt for wheel velocities of 25 m/s. The three alloys synthesized have nominal compositions of  $(\text{Co}_{0.85}\text{Fe}_{0.15})_{88-X}\text{Ni}_X\text{Zr}_7\text{B}_4\text{Cu}_1$  with  $X_{\text{Ni}}=0$  and  $X_{\text{Ni}}=4.4$  and  $(\text{Co}_{0.88}\text{Fe}_{0.12})_{79.4}\text{Nb}_{2.6}\text{Si}_9\text{B}_9$ . The results focus on the  $X_{\text{Ni}}=4.4$  composition but the conclusions are also

qualitatively valid for the  $X_{\text{Ni}}=0$  alloy. As-cast amorphous alloys were wound into toroidal cores and annealed at temperatures ranging from 350–530 °C for 1 h with transverse magnetic field annealed (TMF) or without no field annealed (NF) an applied 2 T transverse magnetic field that was applied during heating and cooling as well. Below, field annealed ribbons treated at temperatures sufficiently high to undergo crystallization will be referred to as field crystallized (FC). Field annealed ribbons treated at lower temperatures such that they remain amorphous will be referred to as field annealed amorphous (FA). High temperature magnetization measurements were made using a Lakeshore high temperature vibrating-sample magnetometer (VSM) with a heating rate of approximately 5 °C/min on average. Core losses and  $B$ - $H$  loops were obtained for toroidal cores with a Walker AMH-401 ac permeameter. Saturation magnetostriction was measured with strain gages by the Wheatstone bridge method with a DMD-21 digital strain meter.

Figure 1 shows an  $M(T)$  plot of the as-cast amorphous ribbons. Several characteristic phase transformation temperatures are identified from these  $M(T)$  plots for the Co–Fe–Zr–B based alloys.<sup>5</sup> These temperatures correspond to (1) primary crystallization temperature of a nanocrystalline phase ( $T_{x1}$ ), (2) secondary crystallization of the remaining amorphous phase ( $T_{x2}$ ), (3) the onset of the formation of fcc  $\gamma$  phase ( $T_{\gamma\text{start}}$ ), (4) the completion of the bcc to fcc transformation ( $T_{\alpha\rightarrow\gamma\text{finish}}$ ), and (5) the Curie temperature of the crystalline fcc phase ( $T_{\text{Curie}\gamma}$ ).

For the Zr–B based  $X_{\text{Ni}}=0$  and  $X_{\text{Ni}}=4.4$  alloys, only bcc phase is observed after 1 h isothermal annealing treatments for temperatures near  $T_{x1}$ . In addition,  $T_{\gamma\text{start}}$  is difficult to

<sup>a)</sup>Author to whom correspondence should be addressed. Electronic mail: pohodnic@andrew.cmu.edu.

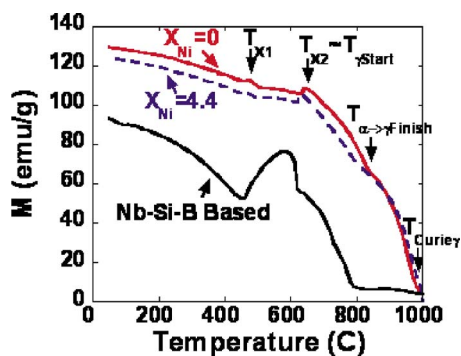


FIG. 1. (Color online)  $M(T)$  curves for  $(\text{Co}_{0.85}\text{Fe}_{0.15})_{88-x}(\text{Ni})_x\text{Zr}_7\text{B}_4\text{Cu}_1$  alloys for  $X_{\text{Ni}}=0$  and  $X_{\text{Ni}}=4.4$  as well as a high field induced anisotropy alloy  $(\text{Co}_{0.88}\text{Fe}_{0.12})_{79.4}\text{Nb}_{2.6}\text{Si}_9\text{B}_9$  for comparison (labeled Nb-Si-B alloy).

identify as it lies close in proximity to  $T_{x2}$ .<sup>5</sup> Based on Fig. 1, the  $X_{\text{Ni}}=4.4$  composition exhibits slightly reduced magnetization in the amorphous and crystallized ribbons and a reduction in  $T_{x2}$ ,  $T_{x1}$ , and  $T_{\alpha \rightarrow \gamma \text{ finish}}$  as compared to  $X_{\text{Ni}}=0$ . The saturation induction of the as-cast amorphous and crystallized ribbons and the Curie temperature of the as-cast ribbon are all significantly smaller for the Nb-Si-B based alloy as compared to the Zr-B based alloys. However, Curie temperature of the as-cast amorphous ribbons cannot be accurately estimated as they lie above  $T_{x1}$ .

Figure 2 illustrates the dynamic  $B$ - $H$  loops obtained at  $f=3$  kHz for ribbons of composition  $X_{\text{Ni}}=4.4$  annealed with (TMF) and without (NF) a 2 T applied transverse magnetic field for 1 h at (a) 350 °C and (b) 530 °C.  $B$ - $H$  loops measured for the Co-Fe-Nb-Si-B alloy are presented in Figs. 2(c) and 2(d) for comparison. X-ray diffraction reveals that both compositions are amorphous after the 350 °C treatment (FA) and that primary crystallization of a bcc nanocrystalline phase has occurred for the 530 °C treatment (FC). The shearing of the hysteresis loops is a result of the induced magnetic anisotropy from transverse magnetic field annealing. The anisotropy field ( $H_K$ ) is estimated from Fig. 2 by extrapolating the linear portion of the hysteresis loop to the saturation induction. An estimate for the field induced uniaxial anisotropy constant  $K_U$  is obtained using  $H_K M_s / 2$ .  $M_s$  is the saturation magnetization of the ribbon. The estimated values of  $H_K$  from the  $B$ - $H$  loops are indicated by arrows in Fig. 2.

The relative areas of the dynamic  $B$ - $H$  loops of Fig. 2 show that the FC Co-Fe-Zr-B based ribbon ( $T=530$  °C,  $X_{\text{Ni}}=4.4$ ) exhibits dramatically higher core losses than the FA Co-Fe-Zr-B based ribbon ( $T=350$  °C,  $X_{\text{Ni}}=4.4$ ). The FC ribbon also exhibits a lower anisotropy field and a lower value of  $K_U$  than the FA ribbon. These trends are illustrated in Fig. 3 for several additional annealing treatments along with the results for the Co-Fe-Nb-Si-B based alloy. For the Co-Fe-Nb-Si-B alloy, the trend in  $H_K$  with annealing temperature is different. The measured values of  $H_K$  are much larger for the FC ribbons as compared to the FA ribbon.

For the  $X_{\text{Ni}}=4.4$  Zr-B based alloy, a sharp increase in  $H_C$  at  $f=3$  kHz and a decrease in  $K_U$  are observed for FC ribbons as compared to FA ribbons. For the Co-Fe-Nb-Si-B alloy, a clear increase in  $K_U$  is observed with increasing annealing temperatures and the increase in  $H_C$  for FC ribbons

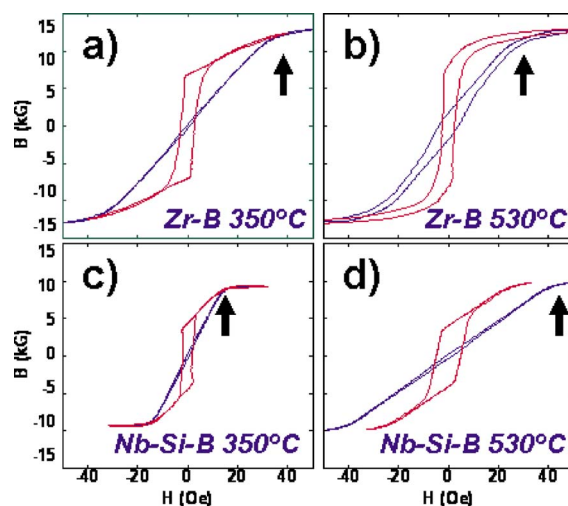


FIG. 2. (Color online) Dynamic  $B$ - $H$  loops obtained for toroidal cores of a Zr-B based alloy with  $X_{\text{Ni}}=4.4$  annealed at (a) 350 °C and (b) 530 °C with and without a field. Dynamic  $B$ - $H$  loops obtained for a Nb-Si-B based alloy annealed at (c) 350 °C and (d) 530 °C with and without a field are presented for comparison. The sheared hysteresis loops correspond to the transverse magnetic field annealed core, and the estimated values of  $H_K$  are indicated by the arrows.

is not as dramatic. The highest values of  $K_U$  measured for the Co-Fe-Nb-Si-B alloy here are lower than, but in reasonable agreement with the values originally quoted in Refs. 7 and 12.

Comparison between the two alloys investigated according to Fig. 3 shows that  $H_C$  is comparable for most of the ribbons investigated with the exception of dramatically higher values measured for the Co-Fe-Zr-B based FC ribbons. In contrast,  $K_U$  is comparable for FC ribbons of both alloys but for the FA ribbons, it is much higher for the Co-Fe-Zr-B based ribbons as compared to the Co-Fe-Nb-Si-B ribbons. Because  $M_s$  is higher for the Co-Fe-Zr-B based ribbons ( $M_s \sim 125$ – $135$  emu/g) than the Co-Fe-Nb-Si-B based ribbons ( $M_s \sim 93$ – $100$  emu/g), they exhibit a higher estimated  $K_U$  for the same measured  $H_K$ .

The trend of increasing  $H_K$  and  $K_U$  with increasing field annealing temperature observed for the Co-Fe-Nb-Si-B alloy here agrees with the results of Yoshizawa *et al.* in Refs. 7 and 12. This trend led the authors to conclude that the large field induced anisotropy is associated with the formation of the nanocrystalline phase. For the Zr-B based alloys studied here, however, the field induced anisotropy is larger for FA ribbons rather than for FC ribbons and the formation of nanocrystalline phase actually results in a decrease in the field induced anisotropy. For the Co-Fe-Zr-B ribbons studied here, it is not yet clear if the amorphous phase plays a significant role in the overall field induced anisotropy. One justification for the possibility of a relatively larger contribution of the amorphous phase to the overall field induced anisotropy for the FC Co-Fe-Zr-B ribbons as compared to the FC Co-Fe-Nb-Si-B ribbons is the relative Curie temperature of the as-cast amorphous ribbons. From Fig. 1, it is observed that the as-cast ribbons of the Co-Fe-Nb-Si-B alloy have a Curie temperature of roughly 500–600 °C which is in the vicinity of the annealing temperatures of 450–550 °C used to obtain FC ribbons. The Co-Fe-Zr-B

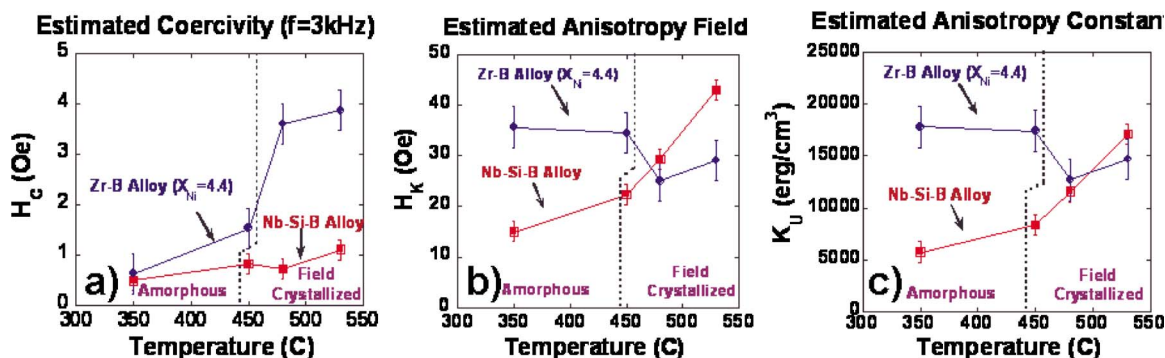


FIG. 3. (Color online) The (a) coercivity, (b) anisotropy field, and (c) field induced anisotropy constant estimated from the 3 kHz dynamic  $B$ - $H$  loop.

as-cast amorphous ribbons, however, have Curie temperatures significantly larger than 600 °C.

Core losses obtained for fixed  $B_{\max}$  of 1, 3, and 10 kG are shown in Fig. 4 for the  $X_{\text{Ni}}=4.4$  Co-Fe-Zr-B based cores annealed at two different temperatures,  $T=350$  °C (FA) and  $T=530$  °C (FC), with and without a transverse field. The core losses were reduced significantly in both cases by transverse field annealing. The FA ribbon also exhibits lower core losses than the FC ribbon in agreement with the coercivity trend of Fig. 3. Core loss results for the Co-Fe-Nb-Si-B alloy are not presented here for brevity.

Possible reasons for the higher dynamic coercivity ( $f=3$  kHz) and higher core losses observed for the FC  $X_{\text{Ni}}=4.4$  Co-Fe-Zr-B based ribbons as compared to the FC Co-Fe-Nb-Si-B alloy include differences in the magnetocrystalline anisotropy of the crystalline grains, the average grain size, and the magnetostriction of the ribbons. For the Co-Fe-Zr-B based  $X_{\text{Ni}}=0$  FC ribbon ( $T=530$  °C),  $\lambda_s > 27$  ppm, and for the corresponding Co-Fe-Nb-Si-B based FC ribbon,  $\lambda_s \sim 8$ –9 ppm. The higher core losses of the Co-Fe-Zr-B FC ribbons may be partially explained by residual stresses in the ribbon and a higher saturation magnetostriction. However, it is not clear if magnetoelastic effects are the dominant cause of the relatively large core losses and coercivity for the field crystallized Co-Fe-Zr-B alloys studied here.

In conclusion, a two phase mixture of amorphous phase and bcc nanocrystalline phase was present in all ribbons investigated in this work after primary crystallization. The Co-Fe-Nb-Si-B alloy first investigated by Yoshizawa *et al.*<sup>7,12</sup> exhibited the largest field induced anisotropy in the field

crystallized state ( $K_U \sim 800$ – $1800$  J/m<sup>3</sup>,  $H_C \sim 0.5$ – $1$  Oe). The origin of the large field induced anisotropy is attributed primarily to the formation of nanocrystalline phase for this composition. However, the largest field induced anisotropy and best soft magnetic properties for the Co-Fe-Zr-B alloys of similar Co:Fe ratio were observed in field annealed amorphous ribbons ( $K_U \sim 1700$ – $2000$  J/m<sup>3</sup>,  $H_C \sim 0.5$ – $1.5$  Oe) rather than field crystallized ribbons. For these compositions, the possibility of a significant contribution of the amorphous phase to  $K_U$  of field crystallized ribbons cannot be excluded based on the data obtained here. The relative Curie temperatures of the as-cast amorphous ribbons of both alloys as compared to the annealing temperatures during field crystallization experiments also suggest that the amorphous phase could provide a relatively larger contribution to the overall  $K_U$  in field crystallized Co-rich alloys of the Co-Fe-Zr-B type. The transverse field annealed amorphous Co-Fe-Zr-B alloys studied here appear to be more attractive for applications requiring low permeability,  $B$ - $H$  linearity to high fields, and low core losses at high frequencies as compared to the corresponding field crystallized Co-Fe-Zr-B alloys. The transverse field annealed Co-rich amorphous Co-Fe-Zr-B alloys investigated here also exhibited properties that are competitive with the field crystallized Co-rich Co-Fe-Nb-Si-B alloys of Yoshizawa *et al.*<sup>7,12</sup>

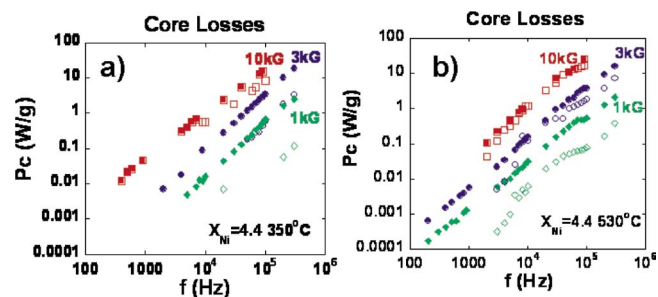


FIG. 4. (Color online) Core loss data for fixed  $B_{\max}$  values of 10, 3, and 1 kG of varying frequency for the (a) 350 °C and (b) 530 °C cores annealed with (open symbols) and without (solid symbols) a transverse magnetic field  $H=2$  T applied. In both cases, the cores annealed with a transverse field exhibit lower core losses.

<sup>1</sup>G. Herzer, *IEEE Trans. Magn.* **26**, 1397 (1990).

<sup>2</sup>Y. Yoshizawa and K. Yamuchi, *Magnetic Properties of Nanocrystalline Fe-Based Soft Magnetic Alloys*, MRS Symposia Proceedings No. 232 (Materials Research Society, Pittsburgh, 1991), pp. 183–192.

<sup>3</sup>K. Suzuki, N. Kataoka, A. Inoue, A. Makino, and T. Masumoto, *Mater. Trans.*, *JIM* **31**, 743 (1990).

<sup>4</sup>M. A. Willard, D. E. Laughlin, M. E. McHenry, D. Thoma, K. Sickafus, J. O. Cross, and V. G. Harris, *J. Appl. Phys.* **84**, 6773 (1998).

<sup>5</sup>P. R. Ohodnicki, S. Y. Park, H. K. McWilliams, K. Ramos, D. E. Laughlin, and M. E. McHenry, *J. Appl. Phys.* **101**, 09N108 (2007).

<sup>6</sup>M. A. Willard, T. M. Heil, and R. Goswami, *Metall. Mater. Trans. A* **38**, 725 (2007).

<sup>7</sup>Y. Yoshizawa, S. Fujii, D. H. Ping, M. Ohnuma, and K. Hono, *Scr. Mater.* **48**, 863 (2003).

<sup>8</sup>M. A. Willard, J. H. Claassen, R. M. Stroud, and V. G. Harris, *J. Appl. Phys.* **91**, 8420 (2002).

<sup>9</sup>X. B. Liang, T. Kulik, J. Ferenc, M. Kowalczyk, G. Vlasak, W. S. Sun, and B. S. Xu, *Physica B* **370**, 151 (2005).

<sup>10</sup>M. A. Willard, J. H. Claassen, and V. G. Harris, *Proceedings of the First IEEE Conference on Nanotechnology*, 2001 (unpublished), pp. 51–55.

<sup>11</sup>M. Kopcewicz, J. Kalinowska, and J. Latuch, *Hyperfine Interact.* **165**, 189 (2005).

<sup>12</sup>Y. Yoshizawa, S. Fujii, D. H. Ping, M. Ohnuma, and K. Hono, *Mater. Sci. Eng., A* **375**–**377**, 207 (2004).